



Preparation of nZVI/MCM-41/rGO for efficient adsorption of cadmium ions from aqueous solution

Mingyue Piao^{a,b}, Xue Peng^c, Huishi Du^d, Hongxue Du^a, Wei Zhang^e, Yuwei Sun^{a,b},
Honghui Teng^{a,b,*}

^aKey Laboratory of Environmental Materials and Pollution Control, Education Department of Jilin Province, College of Engineering, Jilin Normal University, 1301 Haifeng Road, Siping 136000, China, email: tenghonghui@163.com (H. Teng)

^bCollege of Engineering, Jilin Normal University, Siping, China

^cHydrology and Water Resources Bureau of Jilin Province, Siping, China

^dCollege of Tourism and Geographical Science, Jilin Normal University, Siping, China

^eCollege of Chemistry, Jilin Normal University, Siping, China

Received 116 March 2023; Accepted 18 August 2023

ABSTRACT

Cadmium (Cd) emissions have a negative impact on both human health and the environment. Although nano zero-valent iron (nZVI) offers a lot of potential for water pollution treatment, it has been constrained by its instability and ease of aggregation. For the elimination of Cd(II) from aqueous solution, nZVI/MCM supported nZVI (nZVI/MCM-41/rGO) was designed to improve its dispersion and stability. It had a rough, porous structure with apparent Fe⁽⁰⁾ crystallinity and slight rGO crystallinity. On the surface of nZVI/MCM-41/rGO, several oxygen-containing groups were detected. The specific surface area was 15.94 cm²/g, and the pore diameter was concentrated at 23.82 nm. The best performance was occurred at pH 6 with an adsorbent dosage of 2 g/L, and a maximum adsorption capacity of 31 mg/g was achieved after 600 min. Cd(II) removal process was well fitted with second-order kinetic, Langmuir and Freundlich isotherm. The thermodynamic parameter was also analyzed and proved that it was an endothermic ($\Delta H^\circ > 0$) and spontaneous ($\Delta G^\circ < 0$) progress. During adsorption, the crystal type and functional groups of nZVI/MCM-41/rGO did not change, but Fe⁽⁰⁾ was oxidized.

Keywords: Adsorption characteristic; Heavy metal; Composite adsorbent

1. Introduction

One of the biggest environmental problems in the globe is heavy metal contamination. Among them, cadmium (Cd) is extremely poisonous and may be dangerous to organisms and plants [1–3]. Due to its inability to degrade and tissue accumulation, Cd can easily enter food chains, and its effects are amplified with high metal concentrations and continuous exposure. It also contribute to major public health issues such as diabetes [4,5], cellular damage [6], and cancer [7,8]. It is listed as a ‘Priority Regulated Pollutant’ by

the US Environmental Protection Agency because it is carcinogenic. Wastewater containing Cd primarily comes from the mining, smelting, Cd compound, battery, and electroplating industries. Surface waters have been severely contaminated as a result of poor wastewater management [9]. The mean Cd content in sediment of the Xiangjiang River, the primary river in the Dongting Lake Basin, is 25.47 times higher than background levels [10]. Cd concentration in wastewater should be no more than 0.1 mg/L, and that is 0.005 mg/L for drinking water in China. In order to ensure the effluent quality of industrial wastewater and improve

* Corresponding author.

the condition of surface water environment, it is of great significance to adopt effective pollution treatment technology to remove Cd from industrial wastewater. Several removal techniques have been developed, with the ability to effectively remove Cd from aqueous environment, such as electrocoagulation [11], microbial induced carbonate precipitation [12], and phytoremediation [13]. However, there are also problems, such as expensive costs, difficult working conditions, and environmental risks related to chemical use. These disadvantages have limited their prospective uses.

Adsorption is a straightforward and appealing process that has the benefits of great effectiveness, low cost, and no byproducts. As a result, the preparation of functional adsorbents like MoS₂ [14], montmorillonite [15], biochar [16–21], metal–organic frameworks [22], and sodium alginate hydrogel [23], and many others, has received a lot of interest. We are aware that iron-based materials have little influence on the environment, and their huge abundances account determine their relatively low market prices. One of the most popular materials for removing metal ions is nano zero-valent iron (nZVI), which has been widely used for the treatment of Cd in water [24], soil [25], and groundwater [26]. Although nZVI has a lot of potential for treating pollutants, its surface was easily oxidized to generate an iron oxide layer because of its strong reactive activity. Moreover, it is easy to form conglomerations. The Fe–Cd complex formed during Cd adsorption by nZVI is frequently unstable, which significantly lowers the removal effectiveness of Cd and restricts its use [27]. Hence, it is essential to increase the stability of immobilized Cd while enhancing nZVI's capacity for heavy metal removal. According to previous researches, designing composite adsorbent achieved encouraging results in Cd(II) removal in a continuous system [28,29]. Graphene oxide (GO) can serve as a suitable supporting because of its high surface area, low mass, and a variety of functional groups, including carboxyl, hydroxyl, and epoxy groups, which can provide attachment sites for nZVI. MCM-41, a kind of mesoporous silica, has substantial thermal stability, excellent surface area, highly oriented porous structures, and dominant active silanol groups, which make it valuable for adsorption.

In this research, nZVI/MCM-41/rGO was prepared and investigated for the removal of Cd(II) from aqueous solution. Scanning electron microscopy (SEM), Brunauer–Emmett–Teller (BET), X-ray diffraction (XRD), and Fourier-transform infrared spectroscopy (FTIR) were used to thoroughly examine the composition and morphology of the produced composites. The adsorption capacities were examined, and the kinetic, isotherm, and thermodynamic modeling were also studied.

2. Materials and methods

2.1. Materials and chemicals

Graphite, potassium persulfate (K₂S₂O₈), phosphorus pentoxide (P₂O₅), ethyl alcohol (C₂H₅OH), potassium permanganate (KMnO₄), hydrogen peroxide (H₂O₂), sodium dodecyl benzene sulfonate (SDBS), tetraethyl orthosilicate (TEOS), ferric sulfate heptahydrate (FeSO₄·7H₂O), potassium borohydride (KBH₄), sulfuric acid (H₂SO₄), and cadmium sulfate (CdSO₄) were purchased from Aladdin Chemical

Co., (China). All the chemicals used in this study were analytical reagent grade without further purification.

2.2. Preparation of nZVI/MCM-41/rGO

FeSO₄·7H₂O was dissolved in pure water and then C₂H₅OH was added in order to isolate air. By reacting with excessive KBH₄, black particles Fe⁽⁰⁾ was obtained due to reduction action of Fe (II). After an hour oscillation, excessive SDBS was added to clad Fe⁽⁰⁾. The prepared nZVI was transferred into a water bath of 80°C and adjusted to alkaline condition. TEOS was added to react with surplus SDBS to form MCM-41. Three hours later, they were shifted into a reaction kettle to crystallized for 24 h. After completely washing, the obtained powder was put into furnace tube with 600°C for calcining 6 h to form holes in the surface of MCM-41. The obtained nZVI/MCM-41 was mixed with GO which was prepared following the modified method of Hummers [30]. Then KBH₄ was used for reducing GO to rGO. After sufficient washing, nZVI/MCM-41/rGO was stored in cool and dry condition. Molar ratio of SDBS:TEOS:H₂O:FeSO₄·7H₂O was 0.04:1:207:0.2.

2.3. Characterization of nZVI/MCM-41/rGO

After being coated with a thin coating of gold, the surface morphology of nZVI/MCM-41/rGO was examined using a SEM (XL30, FEI, USA) at a working voltage of 10 kV. At the N₂ adsorption and desorption analyzer, specific surface area and pore-size distribution were evaluated utilizing BET and Barrett–Joyner–Halenda (BJH) calculation. The crystalline phase was characterized by XRD (D/max-2500, Rigaku, Japan) in a range of 2θ = 5°–80° with Cu Kα radiation (λ = 1.5406 Å, 40 kV, 200 mA). After powderizing the sample and thoroughly combining it with KBr powder, the powder mixture was compressed into a transparent disk. Then an FTIR spectroscopy (Tensor 320, Bruker, German) was used to scan from 4,000 to 400 cm⁻¹ using an average of 16 scans, with a resolution of 1 cm⁻¹.

2.4. Removal of Cd(II) from aqueous solution

Batch tests were carried out to assess Cd(II) adsorption on nZVI/MCM-41/rGO by adjusting adsorbent dosage, solution pH, initial Cd(II) concentration, and solution temperature. In a series of conical flasks, various dosages of nZVI/MCM-41/rGO (from 0.05 to 0.2 g/50 mL of Cd(II) solution) were added to Cd(II) solution (20–80 mg/L). The pH was adjusted to 3.0–6.0. The Cd(II) solutions were then shaken for 0.5–24 h in 20°C–60°C with a stirring speed of 200 rpm. The best tests were conducted by continuously agitating in 20°C while mixing 100 mg of nZVI/MCM-41/rGO with Cd(II) (C = 50 mg/L, V = 50 mL, and pH = 6). Following the tests, a 0.45 μm syringe filter was used to filter each solution in the treatment group. Flame atomic absorption spectroscopy (AAS-703, PerkinElmer, USA) was used to detect the concentration of Cd(II). The equilibrium adsorption capacity (q_e, mg/g) was calculated according to Eq. (1).

$$q_t = \frac{(C_0 - C_t) \times V}{m} \quad (1)$$

where q_t (mg/g) is adsorption capacity, C_0 (mg/L) is the initial concentration of Cd(II), C_t (mg/L) is the concentration of Cd(II) after t hours adsorption, V (mL) is the volume of Cd(II) solution, and m (mg) is the mass of nZVI/MCM-41/rGO.

2.5. Modeling approach

In order to investigate the rate constant, adsorption process was analyzed using the most often applied kinetic models: pseudo-first-order and pseudo-second-order models. The pseudo-first-order model is written by Eq. (2):

$$\ln(q_e - q_t) = \ln q_e - k_1 t \quad (2)$$

where q_t and q_e (mg/g) are the amounts of Cd(II) adsorbed on nZVI/MCM-41/rGO at any time and equilibrium time, respectively, k_1 (1/min) is the rate constant of the pseudo-first-order. q_e and k_1 are calculated from the intercept and slope of the plots of $\log(q_e - q_t)$.

The pseudo-second-order model is presented by Eq. (3):

$$\frac{t}{q_t} = \frac{1}{k_2 q_e^2} + \frac{t}{q_e} \quad (3)$$

where k_2 (g/(mg·min)) is the rate constant of the pseudo-second-order model.

Intraparticle diffusion model additionally used to portray the transportation of Cd(II) from aqueous solution to nZVI/MCM-41/rGO. The equation of intraparticle diffusion kinetic model can be expressed as in Eq. (4):

$$q_t = k_p t^{0.5} + C \quad (4)$$

where k_p (mg/(g·min^{0.5})) is the rate constant of intraparticle diffusion, and C (mg/g) is the intercept which identified with the thickness of the boundary layer.

The isotherm is the most important parameter in the design of adsorption systems, which explains the relationship between the adsorbent concentration and the adsorption capacity of an adsorbent. Here, Langmuir, Freundlich, Dubinin–Radushkevich, and Temkin were used to determine the best fitting isotherms, which are expressed in Eqs. (5)–(8), respectively.

Langmuir:

$$\frac{1}{q_e} = \frac{1}{q_{\max} K_L} \times \frac{1}{C_e} + \frac{1}{q_{\max}} \quad (5)$$

where q_{\max} (mg/g) corresponds to the maximum adsorption capacity, and K_L (L/g) is the adsorption equilibrium constant.

Freundlich:

$$\ln q_e = \frac{1}{n} \ln C_e + \ln K_F \quad (6)$$

where K_F (mg/g) is the adsorption equilibrium constant, and n corresponds to the number of active sites of nZVI/MCM-41/rGO required for one Cd(II) to adsorb.

Dubinin–Radushkevich:

$$\ln q_e = \ln q_s - K_{\text{ad}} \varepsilon^2 \quad (7)$$

$$\varepsilon^2 = RT \ln \left(1 + \frac{1}{C_e} \right) \quad (8)$$

$$E = (-2K_{\text{ad}})^{-0.5} \quad (9)$$

where q_s (mg/g) is the theoretical isotherm saturation capacity, K_{ad} (mol²/kJ²) is the Dubinin–Radushkevich isotherm constant, R (8.314 J/(mol·K)) is the universal gas constant, T (K) is the solution temperature, and E (kJ/mol) is the adsorption energy.

Temkin:

$$q_e = B \ln A_T + B \ln C_e \quad (10)$$

where B ($=RT/b_T$, J/mol) is Temkin constant related to heat of adsorption, A_T (L/g) is equilibrium binding constant, and b_T is Temkin isotherm constant.

For thermodynamic aspects, adsorption experiments with different initial concentrations of Cd(II) (20, 30, 50, and 60 mg/L) were done in different temperatures (293, 303, and 323 K). Thermodynamic parameters, including changes in Gibbs free energy (ΔG° , kJ/mol), enthalpy (ΔH° , kJ/mol), and entropy (ΔS° , kJ/(mol·K)) were calculated by the following Eqs. (11)–(13):

$$\Delta G^\circ = -RT \ln(K_0) \quad (11)$$

$$\ln K_0 = \frac{\Delta S^\circ}{R} - \frac{\Delta H^\circ}{RT} \quad (12)$$

$$\Delta H^\circ = \Delta G^\circ + T \Delta S^\circ \quad (13)$$

where R (8.314 J/(mol·K)) is the universal gas constant, and T (K) is the solution temperature. K_0 (L/mol) is the ratio of the equilibrium adsorption capacity to the equilibrium Cd(II) concentration.

3. Results and discussions

3.1. Characterization of nZVI/MCM-41/rGO

The prepared MCM-41/rGO was detected as lamellar and wrinkled by SEM analysis as shown in Fig. 1a. After combination with nZVI, it presented porous lamellar structure and the tiny gaps were formed in the surface of nZVI/MCM-41/rGO (Fig. 1b). nZVI entrapped in amorphous MCM-41/rGO caused the surface rough. In Fig. 2, the composite's pore distribution and N₂ adsorption–desorption isotherms were displayed. The quantity of N₂ adsorbed was lower and there was no inflection point when P/P_0 was less than 0.3, indicating a weak force action between rGO and N₂. Adsorption capacity increased with relative pressure increased, suggesting that the surface of nZVI/MCM-41/rGO had many filling holes. Additionally, type IV adsorption isotherms with H₃ hysteresis loops were visible in N₂ adsorption–desorption curves, indicating the existence of mesopores [31]. According to BJH calculations, the prepared nZVI/MCM-41/rGO had a specific surface area of

15.94 cm²/g, a total pore volume of 0.0461 cm³/g, and an average pore width of 23.82 nm.

XRD is widely used as an effective method to assess the crystallinity of diverse materials. Fig. 3a shows different XRD spectra according to different amount of Fe added (SDBS: TEOS:H₂O:FeSO₄·7H₂O = 0.04:1:206.97:x, x = 0.6, 0.3, 0.2, 0.15, 0.13, corresponding to 80%, 60%, 40%, 20% and 10% of iron content, respectively). As presented in Fig. 3a, composites displayed a prominent diffraction peak with a center angle of 2θ = 45°, which was attributed to the (100) crystal plane and was in agreement with α-Fe⁰ (JCPDS card number 006-0696) [32]. A broad and short peak that occurred near 2θ = 24.47° was a sign of rGO sheets [33]. With the increase of Fe⁽⁰⁾ amount, rGO' intensity was weakened and peak width was greatly narrowed down. The functional groups

that were present on the adsorbent surface were identified using FTIR spectroscopy. Fig. 3b reveals the absorbance bands at 3,436; 1,404 and 1,076 cm⁻¹, which indicated the presence of -OH, -COOH, and Si-O [32], respectively. The peak at 1,630 cm⁻¹ was C=C vibration. Peaks at 2,854 and 2,924 cm⁻¹ were -CH₂ stretching vibration bands.

3.2. Adsorption studies

3.2.1. Effect of various factors on adsorption capacity

The pH of the solution is a crucial factor and can affect the degree of ionization, the surface change of the composite, and the charge of Cd(II). There is an optimum pH for the adsorption process due to the competition of proton

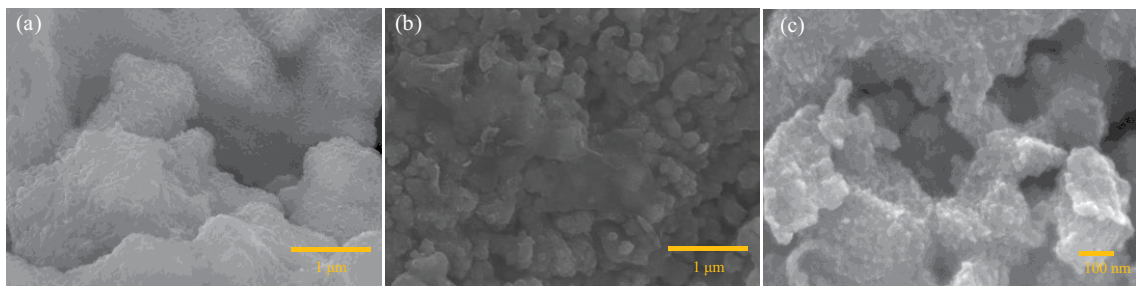


Fig. 1. Scanning electron microscopy photos of (a) MCM-41/rGO and (b, c) nZVI/MCM-41/rGO.

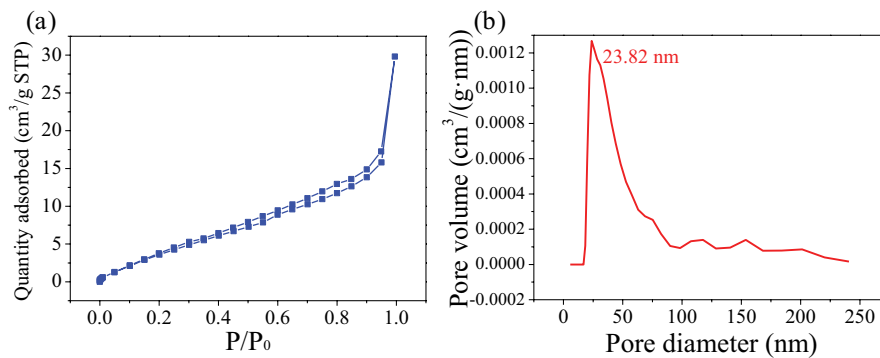


Fig. 2. (a) N₂ adsorption-desorption isotherms and (b) Brunauer-Emmett-Teller pore-size distribution.

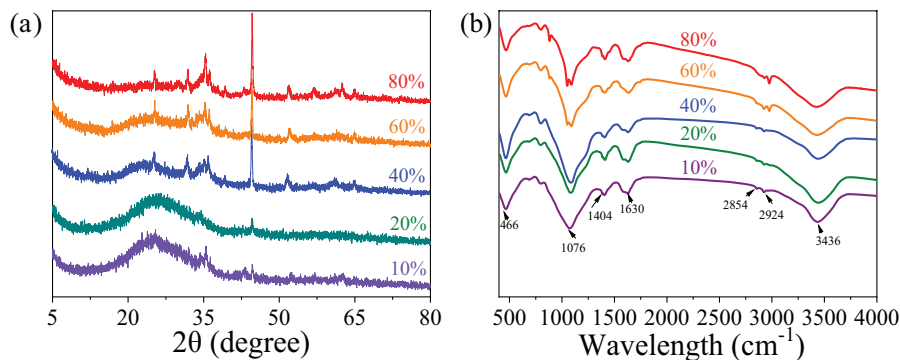


Fig. 3. (a) X-ray diffraction spectra and (b) Fourier-transform infrared spectra of nZVI/MCM-41/rGO.

ions with metallic cations in the lower pH, and precipitation effect at higher basic pH. In order to investigate the effect of pH on Cd(II) adsorption towards the composite, the initial pH of Cd(II) solution was adjusted to 3, 4, 5, and 6. As shown in Fig. 4a, adsorption capacity was increased with pH in acidic condition. According to reports, nZVI's point of zero charge is close to 8 [34], and in every pH tested, nZVI's surface charge was positive. As a result, electrostatic forces between protonated nZVI/MCM-41/rGO and positive metal ions would occur, and H^+ and Cd(II) would compete for active binding sites. The competition between protonated nZVI/MCM-41/rGO and H^+ reduced with higher pH, allowing for chelation and robust coordination with Cd(II).

Fig. 4b provides a description of the dosage's effects on Cd(II) adsorption. The amount of Cd(II) adsorbed on nZVI/MCM-41/rGO were 14.90 ± 0.30 , 19.16 ± 0.13 , 14.77 ± 0.21 and 10.90 ± 0.16 mg/g, corresponding to the dosage 1.0, 2.0, 3.0, and 4.0 g/L, respectively. This might be caused by the lower utilization of adsorption sites and many unoccupied sites remained for higher nZVI/MCM-41/rGO dosage. The maximum adsorption capacity (q_{max}) was 19.16 ± 0.13 mg/g when dosage was 2.0, so 2.0 g/L was chosen for the following tests.

The initial concentration of the adsorbate, one of the most important parameters, might affect the adsorption process. Thus, the impact of the initial Cd(II) concentration was studied and the results are displayed in Fig. 4c. The adsorption capacity dramatically increased as the initial concentration of Cd(II) increased, and q_e were 12.07 ± 0.20 , 13.19 ± 0.24 , 19.16 ± 0.13 , 21.47 ± 0.16 , and 31.30 ± 0.23 mg/g, corresponding to the initial concentration of Cd(II) 20, 30, 40, 50 and 80 mg/L, respectively. A bigger driving force could be produced by the higher starting concentration, which was advantageous for overcoming the mass transfer resistance between the liquid and solid phases.

The enhanced adsorption capacity with temperature is seen in Fig. 4d, where the values of q_e were 8.35 ± 0.13 , 8.03 ± 0.18 , 15.86 ± 0.21 , and 19.15 ± 0.22 mg/g, respectively, for 293, 303, 323, and 333 K. This indicated that Cd(II) adsorption was an endothermic process. Temperature rose made it simpler for Cd(II) in solution to go through Brownian motion, which resulted in easier contact with nZVI/MCM-41/rGO, and in turn enhanced the adsorption capacity. Additionally, due to the fact that rising temperature caused the solution's viscosity decreased, the diffusion of Cd(II) into the interior structure of nZVI/MCM-41/rGO through the outside boundary layer can be accelerated [35].

Comparing nZVI/MCM-41/rGO with other Cd(II) adsorbents, as shown in Table 1, nZVI/MCM-41/rGO demonstrated typical performance.

3.2.2. Cd(II) adsorption kinetics

The characteristic parameters of each kinetic models and their corresponding correlation coefficients are presented in Table 2. According to the correlation coefficients, the pseudo-second-order model (model fitting data is shown in Fig. 5b) fitted the experimental data more closely than the pseudo-first-model did (Fig. 5a), because R^2 was closer to 1, indicating that the rate of sites occupation on nZVI/MCM-41/rGO was proportional to the square of the number of unoccupied sites. Additionally, the calculated q_e ($q_{e,cal}$) obtained with pseudo-second-order kinetic model was agreed with the experimental q_e ($q_{e,exp}$) more consistently. Intraparticle diffusion model is shown in Fig. 5c, and the plotted curves for the uptake of Cd(II) by nZVI/MCM-41/rGO did not pass through origin point, indicating that the adsorption process consisted of two or more steps. Due to the limited diffusion rate within particles, the intraparticle

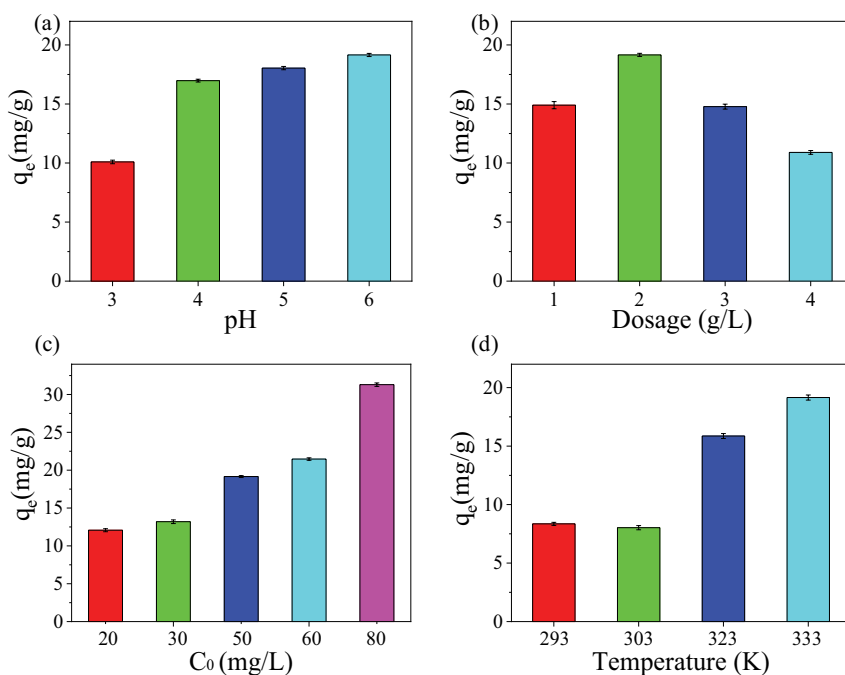


Fig. 4. Effects of (a) pH, (b) dosage, (c) initial concentration of Cd(II), and (d) temperature on adsorption capacity.

Table 1
Cd(II) adsorption capacities by various adsorbents

Adsorbents	q_{\max} (mg/g)	Equilibrium time (min)	Experimental conditions				References
			Initial concentra- tion (mg/L)	pH	Temperature (°C)	Dosage (g/L)	
Sulfide-modified nZVI	104.7	90	40	5.3	25	0.6	[27]
Modified zeolite/nZVI	20.6	120	42.5	4.3	15, 25, and 35	/	[32]
Alginate/gelatin@biochar	86.3	600	50	7	40	1.0	[34]
Biochar	17.8	/	25	/	/	/	[36]
Bio-functional rGO	84.8	60	10	/	30	0.5	[37]
NiO@ γ -Al ₂ O ₃	160.1	120	100	6–7	25	1.5	[38]
β -cyclodextrin/MCM-48	152.2	600	50	7	30	0.2	[39]
Chitosan/MCM-48	122.4	480	50	7	30	0.2	[39]
LaFe@chitosan	35.5	240	1.0	6.5	25	0.5	[40]
SnO ₂ -formaldehyde-chitosan	6.7	0.25	1120	7.0	20–90	1.0	[41]
Chitosan-based hydrogel	234.8	1,440	100	6	70	2.0	[42]
Polyacrylic acid-based hydrogel	197.9	1,440	100	6	70	2.0	[42]
Metal–organic frameworks (UiO-66-SO ₃ H)	194.9	160	40	6	25	/	[43]
nZVI/MCM-41/rGO	31.3	600	80	6	20	2.0	This work

'/': not mentioned in the related article.

Table 2
Adsorption kinetic parameters

Temperature (K)	$q_{e,exp}$ (mg/g)	Pseudo-first-order			Pseudo-second-order		
		$q_{e,cal}$ (mg/g)	$k_1 \times 10^{-2}$ (1/min)	R^2	$q_{e,cal}$ (mg/g)	$k_2 \times 10^{-2}$ (g/(mg·min))	R^2
293	8.7	5.7	0.13	0.7628	8.9	0.065	0.9357
303	9.3	4.0	0.11	0.9756	9.9	0.078	0.9428
323	17.9	5.7	0.14	0.7583	18.0	0.095	0.9973

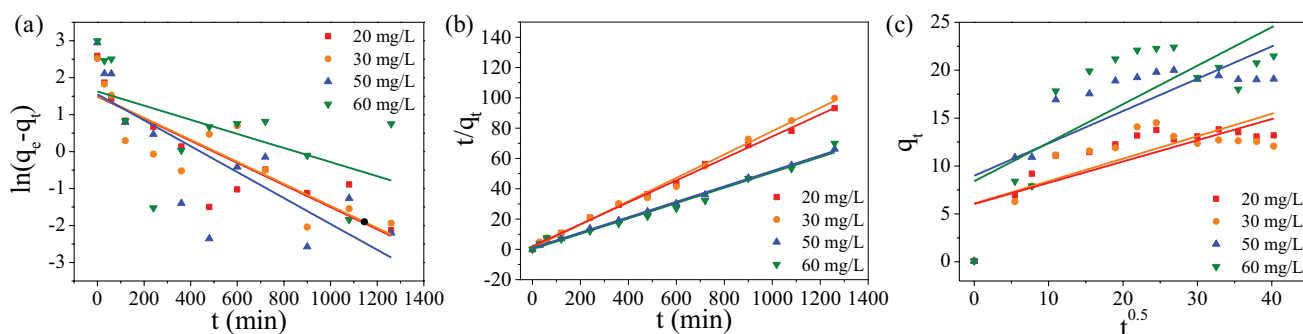


Fig. 5. (a) Pseudo-first-order model, (b) pseudo-second-order model, and (c) intraparticle diffusion model.

diffusion began from the rapid adsorption stage to a gradual adsorption stage. It then reached the final equilibrium stage, during which diffusion within particles was further decreased. Consequently, two or more adsorption mechanisms involved in the removal of Cd(II) by nZVI/MCM-41/rGO, indicating that the adsorption process was not limited to the diffusion of Cd(II) only, but jointly controlled by more than one adsorption stages [37].

3.2.3. Adsorption isotherm

Isotherm parameters were calculated from linear regression curve (Fig. 6) and the results were shown in Table 3. The adsorption of Cd(II) suited well to the Freundlich model according to the correlation coefficient, indicating that adsorption process underwent chemical reactions, and the mechanism of Cd(II) adsorption was the interaction between

Table 3
Isotherm model parameters

Temperature (K)	Langmuir					Freundlich					Dubinin-Radushkevich					Temkin						
	q_{max} (mg/g)	$K_L \times 10^{-3}$ (L/g)	R_L (mg/L)	R^2	RMSE	χ^2	K_F (mg/g)	$1/n$	R^2	RMSE	χ^2	q_s (mg/g)	$K_{ad} \times 10^{-2}$ (mol ² /kJ ²)	R^2	E (kJ/mol)	RMSE	χ^2	A_T (L/g)	B	R^2	RMSE	χ^2
293	34.4	6.4	0.19	0.8812	0.05674	0.01556	0.12	1.3	0.8988	0.1161	0.02140	21.6	1.06	0.7916	6.9	0.4063	0.1088	0.12	7.1	0.8967	1.8619	0.8139
303	27.0	16.4	0.070	0.9415	0.02075	0.00279	0.62	0.8	0.9409	0.0569	0.003812	16.1	0.66	0.8982	8.7	0.1726	0.0165	0.19	5.2	0.9220	1.0898	0.1777
323	31.8	40.9	0.015	0.9402	0.00972	0.00110	2.79	0.5	0.9102	0.0625	0.003762	25.5	0.43	0.9746	10.8	0.0788	0.0025	0.40	6.9	0.9021	1.1999	0.1257

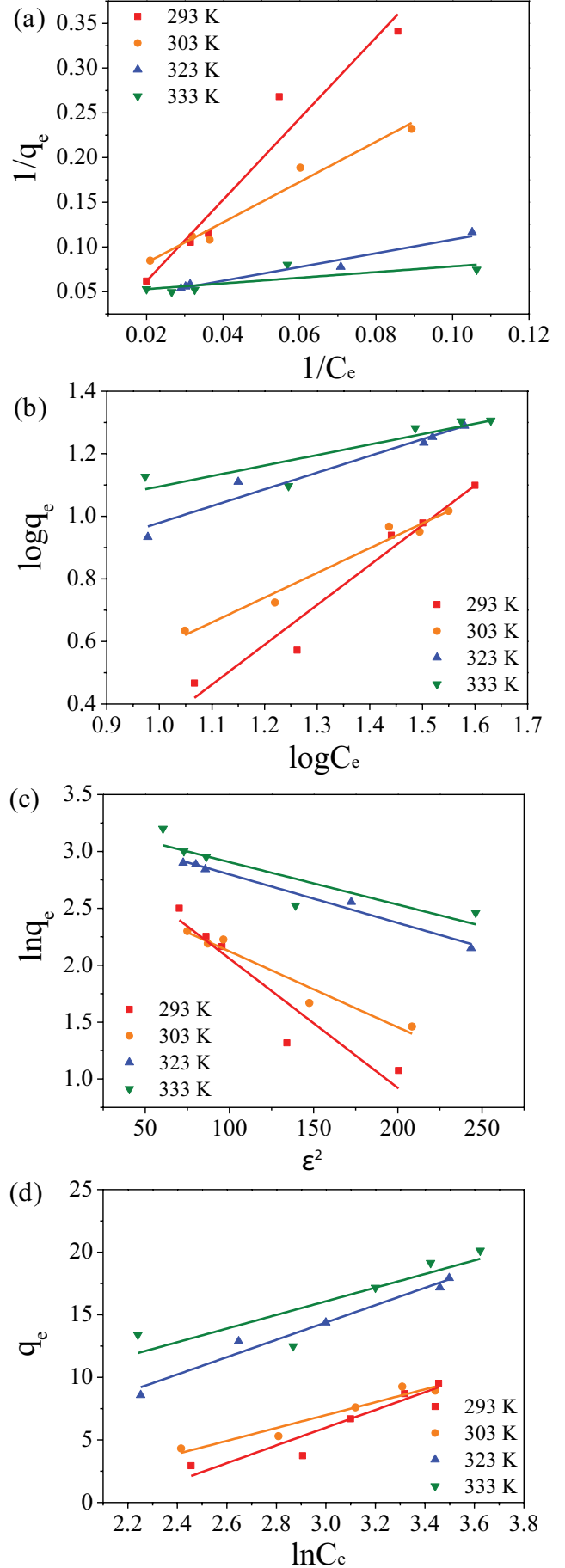


Fig. 6. Isotherm models. (a) Langmuir, (b) Freundlich, (c) Dubinin-Radushkevich, and (d) Temkin.

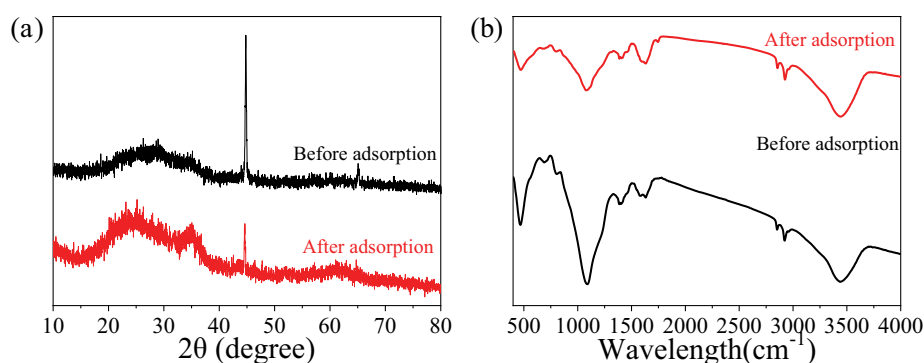


Fig. 7. (a) X-ray diffraction spectra and (b) Fourier-transform infrared spectra before and after adsorption of Cd(II) by nZVI/MCM-41/rGO.

adsorbed Cd(II) molecules on the heterogeneous surfaces of nZVI/MCM-41/rGO. As $1/n$ was smaller than 1 except at 293 K, it is supposed that Cd(II) adsorption behaved favorable adsorption when temperature higher than 293 K. R^2 of Langmuir and Dubinin–Radushkevich were slight lower than that of Freundlich model, but both chi-square (χ^2) and root mean square error (RMSE) were smaller than that of Freundlich, indicating that monolayer physical adsorption and Van der Waals forces were also partially participated in adsorption process. These results proved that the adsorption of Cd(II) on nZVI/MCM-41/rGO was mainly based on monolayer physical adsorption (Van der Waals forces), supplemented by chemical adsorption.

3.2.4. Thermodynamics

The thermodynamic parameters including Gibbs free energy change (ΔG°), entropy change (ΔS°), and enthalpy change (ΔH°) were calculated in three different temperature according to Eqs. (11)–(13). As shown in Table 4, the values of ΔG° were found to be negative, proving that the adsorption process was spontaneous reaction. The positive values of ΔH° reflected an endothermic adsorption, which was the reason for the adsorption capacity increased as increment of the temperature as shown in Fig. 4d. The positive ΔS° indicated the increased randomness at the adsorbate–adsorbent surface during the adsorption progress, and the adsorption of the metal ions proceeded favorably.

3.2.5. Adsorption mechanism

In order to explore the adsorption mechanism, some characterization methods, such as XRD, FTIR, and X-ray photoelectron spectroscopy (XPS) were used. The XRD pattern in Fig. 7a shows that there was no significant increase or decrease in peak after adsorption of Cd(II), indicating that no new crystal was generated during adsorption, and the crystal type of nZVI/MCM-41/rGO did not change. However, the relative strength of the peak representing iron was greatly reduced, indicating that there was a loss of nano iron in the process of adsorption. FTIR spectra as shown in Fig. 7b present that the intensity of broad absorption band at 1,738 cm⁻¹ decreased obviously after Cd(II) adsorption, indicating that C=O may be related to the adsorption

Table 4
Thermodynamic parameters

T (K)	ΔG° (kJ/mol)	ΔH° (kJ/mol)	ΔS° (kJ/mol·K)
293	-42.87	435.38	1.632
303	-34.46	421.12	1.50
323	-18.63	226.85	0.76

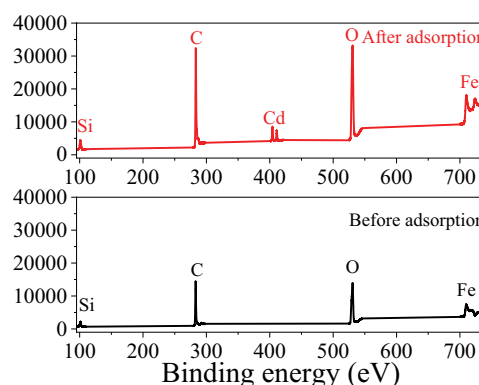


Fig. 8. X-ray photoelectron spectra before and after adsorption of Cd(II) by nZVI/MCM-41/rGO.

process. Also, all the functional groups remained in nZVI/MCM-41/rGO after adsorption, indicating that the chemical composites of the adsorbent were stable. The XPS spectra as shown in Fig. 8 reveal that Cd was successfully adsorbed on nZVI/MCM-41/rGO. It is worth noting that the binding energy of Fe⁽⁰⁾ after adsorption increased from 709.83 to 710.23 eV, indicating that Fe⁽⁰⁾ was oxidized. The binding energy of Si decreased from 101.23 to 100.98 eV, indicating that electrons were obtained after adsorption.

4. Conclusions

nZVI/MCM-41/rGO was fabricated and used for adsorption of Cd(II) from water. The produced adsorbent was porous and rough, with obvious crystallinity of Fe⁽⁰⁾ and limited crystallinity of rGO. Several functional groups, such as -OH, -COOH, and Si-O, were observed. The specific

surface area of nZVI/MCM-41/rGO was 15.94 cm²/g, and average pore diameter was 23.82 nm. The adsorption capacity was increasing with pH and showed best capacity (31.3 mg/g) at pH 6 within 600 min. Experimental data was fitted well with the pseudo-second-order kinetic, Langmuir and Freundlich isotherm models. Thermodynamic parameters reflected an exothermic and spontaneous adsorption progress of Cd(II) towards nZVI/MCM-41/rGO. During adsorption, Fe⁽⁰⁾ was oxidized. It should not be ignored that Fe⁽⁰⁾ contained in nZVI/MCM-41/rGO may leak at lower pH and existed as iron ions, which makes it difficult to reuse. We hope that this study will inspire new adsorbent design that can effectively remove metal ions from water.

Declarations

Ethics approval and consent to participate

Not applicable.

Consent for publication

Not applicable.

Availability of data and materials

Not applicable.

Competing interests

The authors declare that they have no known competing financial interests or personal relationships that could have appeared to influence the work reported in this paper.

Funding

This work was supported by Education Department of Jilin Province of China (JJKH20230518KJ, JJKH20220451KJ), and Department of Science and Technology of Jilin Province of China (20210101398JC, YDZJ202201ZYTS368).

Authors' contributions

Mingyue Piao (writing and funding acquisition), Xue Peng (investigation), Huishi Du (funding acquisition), Hongxue Du (investigation), Wei Zhang (investigation), Yuwei Sun (editing and funding acquisition), Honghui Teng (supervision).

References

- [1] P.G. Peera Sheikh Kulsum, R. Khanam, S. Das, A.K. Nayak, F.M.G. Tack, E. Meers, M. Vithanage, M. Shahid, A. Kumar, S. Chakraborty, T. Bhattacharya, J.K. Biswas, A state-of-the-art review on cadmium uptake, toxicity, and tolerance in rice: from physiological response to remediation process, *Environ. Res.*, 220 (2023) 115098, doi: 10.1016/j.envres.2022.115098.
- [2] Y.X. Hu, H.J. Wu, C.Y. Lu, H.Q. Xu, B.Y. Li, W.C. Guan, M.J. Wu, Y.T. Gao, H.B. Tong, Cadmium chloride exposure impairs the growth and behavior of *Drosophila* via ferroptosis, *Sci. Total Environ.*, 865 (2023) 161183, doi: 10.1016/j.scitotenv.2022.161183.
- [3] L.R. Sun, Y. Mu, L. Xu, X.B. Han, W. Gu, M. Zhang, Transgenerational inheritance of wing development defects in *Drosophila melanogaster* induced by cadmium, *Ecotoxicol. Environ. Saf.*, 250 (2023) 114486, doi: 10.1016/j.ecoenv.2022.114486.
- [4] T. Filippini, L.A. Wise, M. Vinceti, Cadmium exposure and risk of diabetes and prediabetes: a systematic review and dose-response meta-analysis, *Environ. Int.*, 158 (2022) 106920, doi: 10.1016/j.envint.2021.106920.
- [5] S. Saedi, S.E. Watson, J.L. Young, Y. Tan, K.A. Wintergerst, L. Cai, Does maternal low-dose cadmium exposure increase the risk of offspring to develop metabolic syndrome and/or type 2 diabetes?, *Life Sci.*, 315 (2023) 121385, doi: 10.1016/j.lfs.2023.121385.
- [6] V.Souza-Arroyo, J.J. Fabián, L. Bucio-Ortiz, R.U. Miranda-Labra, L.E. Gomez-Quiroz, M.C. Gutiérrez-Ruiz, The mechanism of the cadmium-induced toxicity and cellular response in the liver, *Toxicology*, 480 (2022) 153339, doi: 10.1016/j.tox.2022.153339.
- [7] Z. Khan, A. Elahi, D.A. Bukhari, A. Rehman, Cadmium sources, toxicity, resistance and removal by microorganisms—a potential strategy for cadmium eradication, *J. Saudi Chem. Soc.*, 26 (2022) 101569, doi: 10.1016/j.jscs.2022.101569.
- [8] V.A. Florez-Garcia, E.C. Guevara-Romero, M.M. Hawkins, L.E. Bautista, T.E. Jenson, J. Yu, A.E. Kalkbrenner, Cadmium exposure and risk of breast cancer: a meta-analysis, *Environ. Res.*, 219 (2023) 115109, doi: 10.1016/j.envres.2022.115109.
- [9] S. Illuminati, A. Annibaldi, C. Truzzi, M.-L. Tercier-Waeber, S. Noël, C.B. Braungardt, E.P. Achterberg, K.A. Howell, D. Turner, M. Marini, T. Romagnoli, C. Totti, F. Confalonieri, F. Graziottin, J. Buffle, G. Scarponi, *In-situ* trace metal (Cd, Pb, Cu) speciation along the Po River plume (Northern Adriatic Sea) using submersible systems, *Mar. Chem.*, 212 (2019) 47–63.
- [10] J. Liu, Y. Xu, Y. Cheng, Y. Zhao, Y. Pan, G. Fu, Y. Dai, Occurrence and risk assessment of heavy metals in sediments of the Xiangjiang River, China, *Environ. Sci. Pollut. Res. Int.*, 24 (2017) 2711–2723.
- [11] L. Singh Thakur, R. Baghel, A. Sharma, S. Sharma, S. verma, H. Parmar, A. Kumar Varma, P. Mondal, Simultaneous removal of lead, chromium and cadmium from synthetic water by electrocoagulation: Optimization through response surface methodology, *Mater. Today Proc.*, 72 (2023) 2697–2704.
- [12] M.P. Sheng, D.H. Peng, S.H. Luo, T. Ni, H.Y. Luo, R.F. Zhang, Y. Wen, H. Xu, Micro-dynamic process of cadmium removal by microbial induced carbonate precipitation, *Environ. Pollut.*, 308 (2022) 119585, doi: 10.1016/j.envpol.2022.119585.
- [13] L.A. Feng, B.Y. Liang, X.L. Zeng, C. Shi, H.D. Yin, Y.M. Feng, Y.Q. Chen, Q.L. Yu, Engineered bacterium-binding protein promotes root recruitment of functional bacteria for enhanced cadmium removal from wastewater by phytoremediation, *Water Res.*, 221 (2022) 118746, doi: 10.1016/j.watres.2022.118746.
- [14] S.S. Lv, S.J. Du, X.G. Chen, Y.Y. Liu, G.J. Wang, Z.C. Li, First principles study on the cadmium adsorption behaviour of MoS₂ with structural defects and doping, *Solid State Commun.*, 342 (2022) 114611, doi: 10.1016/j.ssc.2021.114611.
- [15] Z.-l. Zeng, C. Yu, R.-p. Liao, X.Q. Cai, Z.-h. Chen, Z.K. Yu, Z.-x. Wu, Preparation and characterization of sodium polyacrylate grafted montmorillonite nanocomposite for the adsorption of cadmium ions from aqueous solution, *Colloids Surf., A*, 656 (2023) 130389, doi: 10.1016/j.colsurfa.2022.130389.
- [16] Y.J. Xu, H.Y. Xia, Q. Zhang, G.Y. Jiang, W.C. Cai, W.H. Hu, Adsorption of cadmium(II) in wastewater by magnesium oxide modified biochar, *Arabian J. Chem.*, 15 (2022) 104059, doi: 10.1016/j.arabjc.2022.104059.
- [17] Z.Y. Gao, D.X. Shan, J.H. He, T. Huang, Y. Mao, H.P. Tan, H.T. Shi, T.Z. Li, T.P. Xie, Effects and mechanism on cadmium adsorption removal by CaCl₂-modified biochar from selenium-rich straw, *Bioresour. Technol.*, 370 (2023) 128563, doi: 10.1016/j.biortech.2022.128563.
- [18] K. Zhang, Y.Q. Yi, Z.Q. Fang, Remediation of cadmium or arsenic contaminated water and soil by modified biochar: a review, *Chemosphere*, 311 (2023) 136914, doi: 10.1016/j.chemosphere.2022.136914.
- [19] T.Q. Liu, Y. Lawluy, Y. Shi, J.O. Ighalo, Y.D. He, Y.J. Zhang, P.-S. Yap, Adsorption of cadmium and lead from aqueous solution using modified biochar: a review, *J. Environ. Chem. Eng.*, 10 (2022) 106502, doi: 10.1016/j.jece.2021.106502.

- [20] J. Wang, Y. Wang, J. Wang, G. Du, K.Y. Khan, Y. Song, X. Cui, Z. Cheng, B. Yan, G. Chen, Comparison of cadmium adsorption by hydrochar and pyrochar derived from Napier grass, *Chemosphere*, 308 (2022) 136389, doi: 10.1016/j.chemosphere.2022.136389.
- [21] Q.S. Yuan, P.F. Wang, X. Wang, B. Hu, C. Wang, X.L. Xing, Nano-chlorapatite modification enhancing cadmium(II) adsorption capacity of crop residue biochars, *Sci. Total Environ.*, 865 (2023) 161097, doi: 10.1016/j.scitotenv.2022.161097.
- [22] M. Mansoorianfar, H. Nabipour, F. Pahlevani, Y.W. Zhao, Z. Hussain, A. Hojjati-Najafabadi, H.Y. Hoang, R.J. Pei, Recent progress on adsorption of cadmium ions from water systems using metal-organic frameworks (MOFs) as an efficient class of porous materials, *Environ. Res.*, 214 (2022) 114113, doi: 10.1016/j.envres.2022.114113.
- [23] J.P. Li, M.X. Chen, X.Q. Yang, L. Zhang, Preparation of a novel hydrogel of sodium alginate using rural waste bone meal for efficient adsorption of heavy metals cadmium ion, *Sci. Total Environ.*, 863 (2023) 160969, doi: 10.1016/j.scitotenv.2022.160969.
- [24] N.Y. Owija, S.A. Kosa, M. Abdel Salam, Removal of cadmium ions from aqueous solution by zero valent iron nanoparticles: equilibrium and thermodynamic studies, *J. Mol. Liq.*, 342 (2021) 117462, doi: 10.1016/j.molliq.2021.117462.
- [25] D. Yang, J.W. Zhang, S.Y. Yang, Y. Wang, X.J. Tang, J.M. Xu, X.M. Liu, Biochar-supported nanoscale zero-valent iron can simultaneously decrease cadmium and arsenic uptake by rice grains in co-contaminated soil, *Sci. Total Environ.*, 814 (2022) 152798, doi: 10.1016/j.scitotenv.2021.152798.
- [26] I.-G. Song, Y.-G. Kang, J.-H. Kim, H. Yoon, W.Y. Um, Y.-S. Chang, Assessment of sulfidated nanoscale zerovalent iron for *in-situ* remediation of cadmium-contaminated acidic groundwater at a zinc smelter, *J. Hazard. Mater.*, 441 (2023) 129915, doi: 10.1016/j.jhazmat.2022.129915.
- [27] R.Q. Gao, P.W. Hu, Y.N. Dai, Y. Zhang, L. Liu, W.Z. Yang, Removal of cadmium(II) from aqueous solutions by a novel sulfide-modified nanoscale zero-valent iron supported on kaolinite: treatment efficiency, kinetics and mechanisms, *Appl. Surf. Sci.*, 602 (2022) 154353, doi: 10.1016/j.apsusc.2022.154353.
- [28] M.J. Amiri, M. Khozaei, A. Gil, Modification of the Thomas model for predicting unsymmetrical breakthrough curves using an adaptive neural-based fuzzy inference system, *J. Water Health*, 17 (2019) 25–36.
- [29] M.J. Amiri, R. Roohi, A. Gil, Numerical simulation of Cd(II) removal by ostrich bone ash supported nanoscale zero-valent iron in a fixed-bed column system: utilization of unsteady advection-dispersion-adsorption equation, *J. Water Process Eng.*, 25 (2018) 1–14.
- [30] D.C. Marcano, D.V. Kosynkin, J.M. Berlin, A. Sinitskii, Z.Z. Sun, A. Slesarev, L.B. Alemany, W. Lu, J.M. Tour, Improved synthesis of graphene oxide, *ACS Nano*, 4 (2010) 4806–4814.
- [31] V. Ramya, D. Murugan, C. Lajapathirai, S. Meenatchisundaram, S. Arumugam, A composite adsorbent of superparamagnetic nanoparticles with sludge biomass derived activated carbon for the removal of chromium(VI), *J. Cleaner Prod.*, 366 (2022) 132853, doi: 10.1016/j.jclepro.2022.132853.
- [32] S. Tasharofi, Z. Rouzitalab, D.M. Maklavany, A. Esmaeili, M. Rabieezadeh, M. Askarieh, A. Rashidi, H. Taghdisian, Adsorption of cadmium using modified zeolite-supported nanoscale zero-valent iron composites as a reactive material for PRBs, *Sci. Total Environ.*, 736 (2020) 139570, doi: 10.1016/j.scitotenv.2020.139570.
- [33] S. Bagheri, A. Esrafil, M. Kermani, J. Mehralipour, M. Gholami, Performance evaluation of a novel rGO-Fe⁰/Fe₃O₄-PEI nanocomposite for lead and cadmium removal from aqueous solutions, *J. Mol. Liq.*, 320 (2020) 114422, doi: 10.1016/j.molliq.2020.114422.
- [34] J. Fan, Y.H. Guo, J.J. Wang, M.H. Fan, Rapid decolorization of azo dye methyl orange in aqueous solution by nanoscale zerovalent iron particles, *J. Hazard. Mater.*, 166 (2009) 904–910.
- [35] Y.M. Zong, X.X. Wang, H. Zhang, Y. Li, J. Yu, C. Wang, Z.T. Cai, J.C. Wei, L. Ding, Preparation of a ternary composite based on water caltrop shell derived biochar and gelatin/alginate for cadmium removal from contaminated water: performances assessment and mechanism insight, *Int. J. Biol. Macromol.*, 234 (2023) 123637, doi: 10.1016/j.ijbiomac.2023.123637.
- [36] A. Ameen Hezam Saeed, N. Yub Harun, M. Mahmoud Nasef, A. Al-Fakih, A. Abdulhakim Saeed Ghaleb, H. Kolawole Afolabi, Removal of cadmium from aqueous solution by optimized rice husk biochar using response surface methodology, *Ain Shams Eng. J.*, 13 (2022) 101516, doi: 10.1016/j.asej.2021.06.002.
- [37] X.Y. Lin, L. Gan, G. Owens, Z.L. Chen, Removal of cadmium from wastewater using biofunctional reduced graphene oxide synthesized by *Lysinibacillus sphaericus*, *J. Cleaner Prod.*, 383 (2023) 135369, doi: 10.1016/j.jclepro.2022.135369.
- [38] H. Chen, H.N. Wu, N.S.A. Khan, X.M. Peng, F.X. Qiu, T. Zhang, Converting wastes to resource: preparation of NiO@γ-Al₂O₃ sludge composite from aluminum-containing sludge for cadmium removal from wastewater, *J. Cleaner Prod.*, 392 (2023) 136335, doi: 10.1016/j.jclepro.2023.136335.
- [39] Y.L. Jiang, M.R. Abukhadra, N.M. Refay, M.F. Sharaf, M.A. El-Meligy, E.M. Awwad, Synthesis of chitosan/MCM-48 and β-cyclodextrin/MCM-48 composites as bio-adsorbents for environmental removal of Cd²⁺ ions: kinetic and equilibrium studies, *React. Funct. Polym.*, 154 (2020) 104675, doi: 10.1016/j.reactfunctpolym.2020.104675.
- [40] Z.C. Lan, Y. Lin, C.P. Yang, Lanthanum-iron incorporated chitosan beads for adsorption of phosphate and cadmium from aqueous solutions, *Chem. Eng. J.*, 448 (2022) 137519, doi: 10.1016/j.cej.2022.137519.
- [41] M.E. Mahmoud, M.S. Abdelwahab, G.A.A. Ibrahim, The design of SnO₂-crosslinked-chitosan nanocomposite for microwave-assisted adsorption of aqueous cadmium and mercury ions, *Sustainable Chem. Pharm.*, 28 (2022) 100731, doi: 10.1016/j.scp.2022.100731.
- [42] P.B. Vilela, C.A. Matias, A. Dalalibera, V.A. Becegato, A.T. Paulino, Polyacrylic acid-based and chitosan-based hydrogels for adsorption of cadmium: equilibrium isotherm, kinetic and thermodynamic studies, *J. Environ. Chem. Eng.*, 7 (2019) 103327, doi: 10.1016/j.jece.2019.103327.
- [43] S. Gul, Z. Ahmad, M. Asma, M. Ahmad, K. Rehan, M. Munir, A.A. Bazmi, H.M. Ali, Y. Mazroua, M.A. Salem, M.S. Akhtar, M.S. Khan, L.F. Chuah, S. Asif, Effective adsorption of cadmium and lead using SO₃H-functionalized Zr-MOFs in aqueous medium, *Chemosphere*, 307 (2022) 135633, doi: 10.1016/j.chemosphere.2022.135633.